



ORIGINAL ARTICLE

Evaluate the effect of graphitic carbon nitride nanosheets decorated with copper nanoparticles on biofilm and *icaA* gene expression in *Staphylococcus aureus* isolated from clinical samples



Somaye Rashki^a, Mojgan Ghanbari^b, Zainab Hashim Khudhair^c,
Zeynab Marzhoseyni^d, Zakaria Bameri^e, Saleh Afsharikhah^f,
Waleed K. Abdulsahib^g, Ali Nazari-Alam^{h,*}, Masoud Salavati-Niasari^{b,*}

^a Department of Microbiology, Iranshahr University of Medical Sciences, Iranshahr, Iran

^b Institute of Nano Science and Nano Technology, University of Kashan, Kashan, Iran

^c Department of Chemistry, College of Sciences for Women, Babylon University, Hilla, Iraq

^d Department of Microbiology, Kashan University of Medical Sciences, Kashan, Iran

^e Infectious Disease and Tropical Medicine Research Center, Resistant Tuberculosis Institute, Zahedan University of Medical Sciences, Zahedan, Iran

^f Department of Pathobiology, Faculty of Veterinary Medicine, Shahid Bahonar University of Kerman, Kerman, Iran

^g Department of Pharmacology and Toxicology, College of Pharmacy, Al-Farahidi University, Baghdad, Iraq

^h Infection Diseases Research Center, Kashan University of Medical Sciences, Kashan, Iran

Received 31 January 2023; accepted 2 April 2023

Available online 11 April 2023

KEYWORDS

Antimicrobial activity;
Nanostructures;
Cu/g-C₃N₄ nanocomposites;
Antibacterial;
Biofilm

Abstract The emergence, spread, and persistence of multidrug-resistant (MDR) bacteria have become a public health threat. Therefore, it is urgent to investigate novel antimicrobial materials without antibacterial resistance. In this regard, Copper/graphitic carbon nitride nanocomposites (Cu/g-C₃N₄ NCs) with different loading amounts of Cu nanoparticles (NPs) have been successfully prepared via the co-precipitation-sonication approach. The purity of the nanostructures was verified by the X-ray diffraction (XRD) pattern. The antibacterial activity of Cu/g-C₃N₄ NCs versus tested bacteria were determined by the microdilution technique. Inhibition of biofilm formation was also evaluated using the microtiter plate method. In addition, the ability of Cu/g-C₃N₄ NCs to the expression level of the *icaA* gene was assessed by the Real-Time PCR technique. Our results

* Corresponding authors.

E-mail address: salavati@kashanu.ac.ir (M. Salavati-Niasari).

Peer review under responsibility of King Saud University.



showed that the doping of graphitic carbon nitride with Cu-NPs can improve the antibacterial activity of g-C₃N₄. So, sample 4 (Cu:g-C₃N₄ 1;1), with higher Cu content, had the highest antibacterial activity toward tested bacteria. The result also showed that sample 4 recorded the largest inhibition zone diameters against tested bacteria, including *Staphylococcus aureus* (29 mm) and *Pseudomonas aeruginosa* (16 mm). In addition, Cu/g-C₃N₄ NCs exhibited a 65% reduction in biofilm formation for *Staphylococcus aureus*. Moreover, *icaA* gene was down-regulated after treatment with Cu/g-C₃N₄ NCs. In conclusion, our study showed that extract Cu/g-C₃N₄ NCs can use as a promising anti-biofilm agent against biofilm-producing bacteria.

© 2023 The Author(s). Published by Elsevier B.V. on behalf of King Saud University. This is an open access article under the CC BY-NC-ND license (<http://creativecommons.org/licenses/by-nc-nd/4.0/>).

1. Introduction

The emergence of multidrug-resistant organisms is considered one of the principal public health challenges since it has a major impact on human health worldwide and causes an increase in the average length of hospital stays, morbidity, mortality, and healthcare costs. Bacterial resistance to antibiotics can be affected by related genetic changes, the impermeability of the bacteria to the antibiotic, and changing the drug target (Giraldi et al., 2019). Many mechanisms are involved in bacterial resistance to antibiotics. One of the main factors contributing to drug resistance is biofilm formation (Gajdacs et al., 2021). The biofilm formation of bacteria leads to acute infections such as urinary tract infection, otitis media, osteomyelitis, wound infection, endocarditis and cystic fibrosis. These infections are today a major cause of treatment failure. Various genes induced biofilm formation in bacterial isolates. For example, the presence of *icaABCD* locus is an essential factor for biofilm formation in *S. aureus*. So that, this locus induced polysaccharide intercellular adhesin (PIA) expression that plays an important role in the initial attachment and biofilm formation of *S. aureus* (Cucarella et al., 2001). Thus, the decrease in the expression of this locus (*icaA* gene) has an important effect to reduce of biofilm formation. Moreover, several studies have demonstrated a direct connection between antimicrobial resistance and biofilm formation. Bacterial biofilms can be more resistant to antibiotics, compared to the planktonic state (Rashki et al., 2022a). To decrease treatment defeat in these infections, it is necessary to design new promising materials to inhibit biofilm formation. Over the last few decades, nanotechnology has been widely studied in fields such as the treatment of cancer, bacterial infections, and drug delivery. These sciences can have an important role in the development of new materials because of their unique physicochemical characteristics and biomedical applications (Zhang et al., 2013; Abdulhusain et al., 2022; Mahde et al., 2022). In recent years, nanostructure-based antimicrobial has appeared as an encouraging agent for the treatment of bacterial infections. Recently, carbon-based materials have been widely studied in the fields of drug delivery, cancer therapy, and antibacterial (Sert et al., 2021; Thurston et al., 2020). Among these, graphitic carbon nitride (g-C₃N₄) is a class of polymeric materials mainly composed of CN bonds that have emerged as an encouraging prospect for a variety of applications (Naseri et al., 2017). Moreover, g-C₃N₄ has drawn tremendous concentration because of its simple preparation, superior biocompatibility, excellent physicochemical stability, photocatalytic applications, and degradation of pollutants in water (Oves et al., 2020; Wang et al., 2020). However, graphitic carbon nitride (g-C₃N₄) has no inherent antibacterial activity, and therefore cannot be used on its own and its use as antimicrobial agent is limited. To empower graphitic carbon nitride with anti-bacterial properties, new efficient nanomaterials have been designed based on graphitic carbon nitride for antibacterial applications (Huang et al., 2014). Several case studies report that the doping nanomaterials (e.g. GO, TiO₂, Ag, AgBr, etc.) with g-C₃N₄ is the most facile method to improve the antibacterial and antibiofilm

performance of g-C₃N₄ (Ma et al., 2016; Xu et al., 2019; Zhou et al., 2016). In this regard, researchers have shown that several g-C₃N₄-based heterostructures, such as g-C₃N₄/CdS, g-C₃N₄/TiO₂, g-C₃N₄/NaNbO₃, g-C₃N₄/BiOI, g-C₃N₄ nanosheets/Bi₂MoO₆, g-C₃N₄ nanosheet/carbon dots/Ag₆Si₂O₇, g-C₃N₄ nanosheet/MgO, and ZnO/g-C₃N₄ could improve the antibacterial and antibiofilm activities because of their synergistic effect (Deng et al., 2017; Li et al., 2015; Li et al., 2019). Moreover, Murugesan et al. demonstrated that the g-C₃N₄/silver iodide nanocomposite could interfere with the bacterial DNA and disturb the bacterial metabolic pathway as a novel antibacterial agent. This nanocomposite can be used for the growth inhibition of bacteria (Murugesan et al., 2018). For this reason, the preparation of g-C₃N₄-based nanomaterials has been the focus of considerable attention in recent years. In this study, various amounts of Cu NPs were added to g-C₃N₄ dispersion to enhance the antibacterial and antibiofilm performance of g-C₃N₄, which was termed Cu/g-C₃N₄ nanocomposites. In this regard, we introduce a new nanocomposite containing g-C₃N₄ and different contents of copper for its potential as antimicrobial and biofilm agent. Besides, the ability of Cu/g-C₃N₄ NCs to the expression level of the *icaA* gene was evaluated by the Real-Time PCR technique. The preparation of Cu/g-C₃N₄ nanocomposite was confirmed via X-ray diffraction (XRD) and scanning electron microscopy (SEM). Therefore, we speculated that the Cu/g-C₃N₄ nanocomposite with significant antibacterial performance could enhance the clinical application of the g-C₃N₄ nanosheets.

2. Materials and methods

2.1. Materials

All chemical reagents supplied within the analytic standard, copper nitrate 99% Cu (NO₃)₂, and sodium dodecyl sulfate (SDS) ≥ 99, melamine 99.9% (C₃H₆N₆), L-Ascorbic acid > 98% were obtained from Merck and applied without further purification. Also, Mueller Hinton broth and Mueller Hinton agar were acquired from Merck (Germany).

2.2. Synthesis of Cu particle

First, 300 mg of Cu(NO₃)₂·3H₂O was dissolved in 10 ml of deionized water. This solution was agitated for 30 min at 25 °C. After that, 300 mg of SDS was added to the Cu²⁺ solution. Then, ascorbic acid was added dropwise to the above mixture under a stirrer to reduce Cu²⁺ to Cu⁰. The brick-red solution was centrifuged and washed with deionized water. Finally, the prepared particle was dried at 50 °C for 24 h (Begletsova et al., 2018; Cheng et al., 2006).

Gene	Primer sequences	Primer length
icaA	F-3'-ACGTGGCTACTGGGATACTG-5'	21
	R-3'-CTTCAAAGACCTCCAATG-5'	20
glyA	F-3'-GGTGGCTGTGAGTTTGTAGATG-5'	22
	R-3'-CGCTTGTGAACCTGAATGTG-5'	20

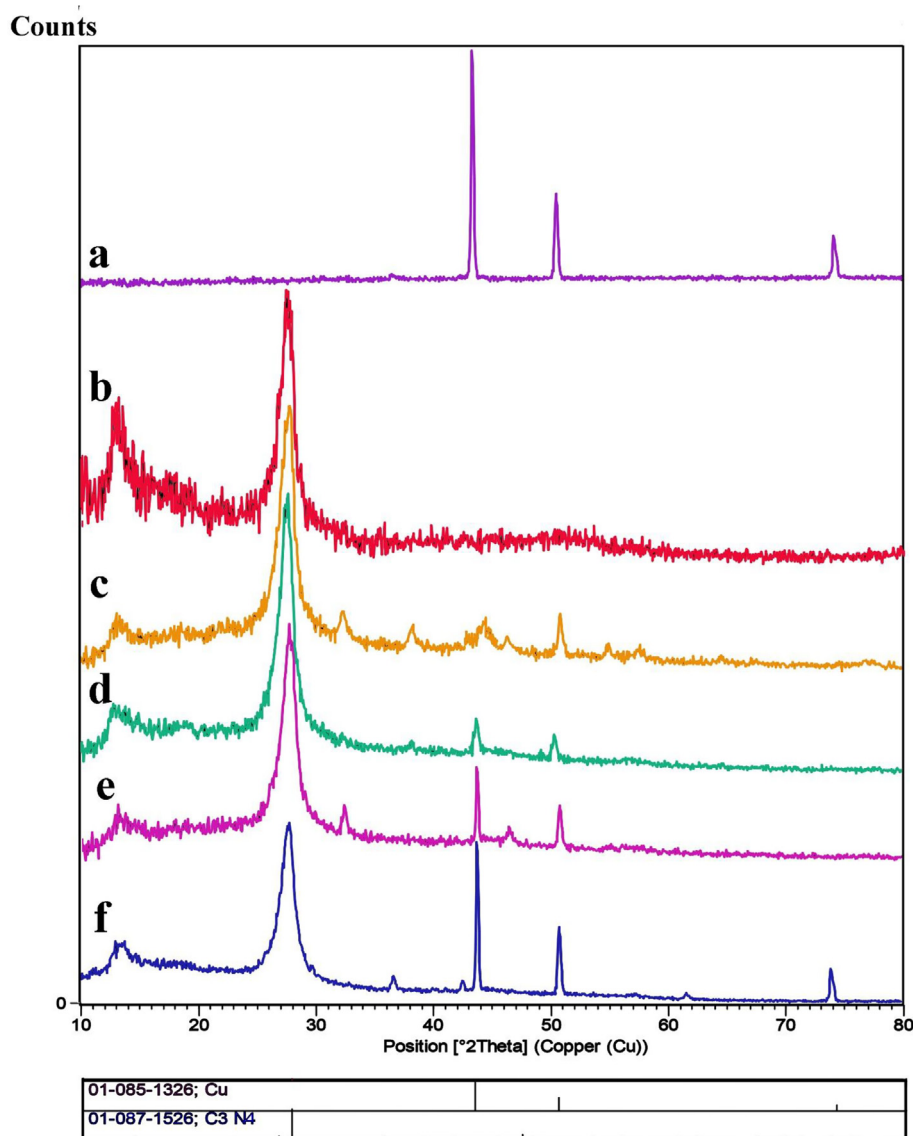


Fig. 1 XRD patterns of a) Cu, b) $g\text{-C}_3\text{N}_4$, c) Cu/ $g\text{-C}_3\text{N}_4$ (0.3:1), d) Cu/ $g\text{-C}_3\text{N}_4$ (0.4:1), e) Cu/ $g\text{-C}_3\text{N}_4$ (0.5:1), and f) Cu/ $g\text{-C}_3\text{N}_4$ (1:1), nanocomposites.

2.3. Preparation of Cu/ $g\text{-C}_3\text{N}_4$ nanocomposites via co-precipitation-sonication method

$g\text{-C}_3\text{N}_4$ was prepared according to our previous paper (Yousefzadeh et al., 2022). In a typical procedure, a specific quantity of melamine (3.0 g) was directly heated at 550 °C

for 4 h. The yellow powder of graphitic carbon nitride was obtained and used for further tests. Then, 300 mg of $g\text{-C}_3\text{N}_4$ was dispersed in 15 ml of deionized water (DIW) for 0.5 h, and the mixture was stirred for 1 h. Next, the various weight ratios of $\text{Cu}(\text{NO}_3)_2$ (mass ratio of Cu: $g\text{-C}_3\text{N}_4$ 0.3:1 (sample 1), 0.4:1 (sample 2), 0.5:1 (sample 3), and 1:1 (sample 4)) were dissolved in 10 ml of DIW and mixed with the $g\text{-C}_3\text{N}_4$ suspen-

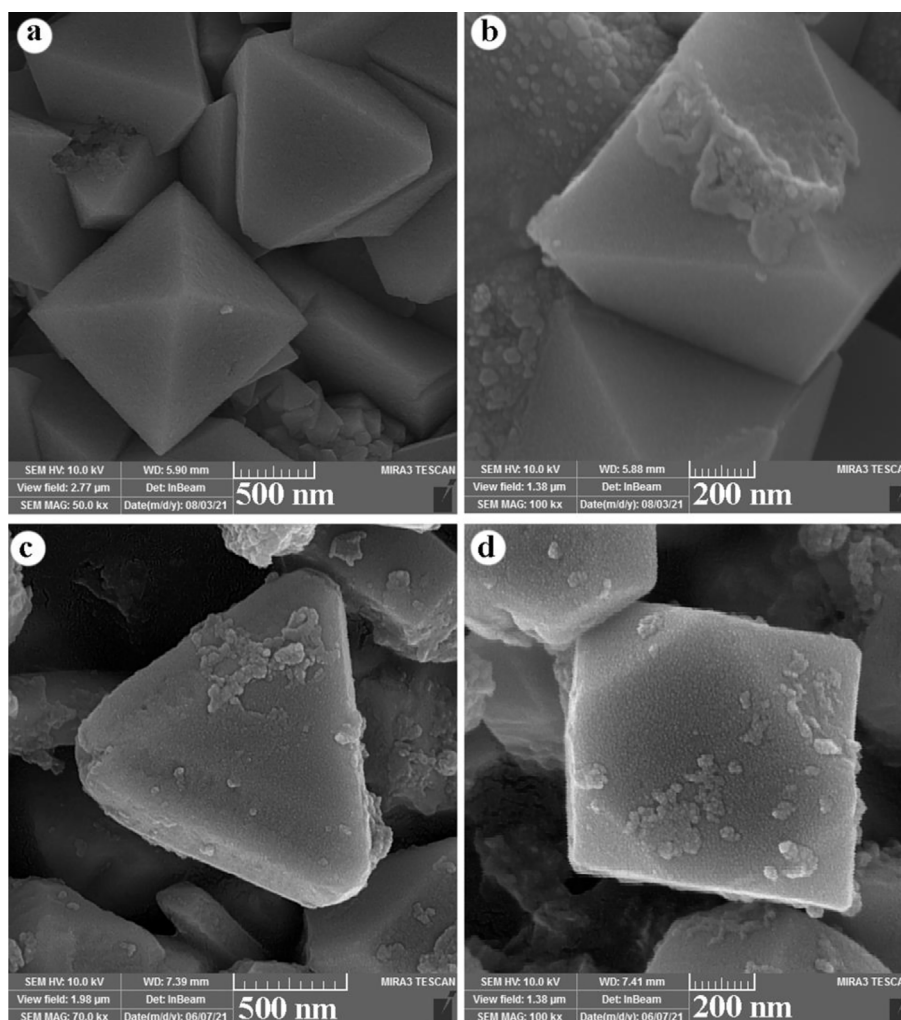


Fig. 2 FESEM images of Cu NPs with (a,b) and without (c,d) SDS.

sion. Then, ascorbic acid was added to suspensions under a stirrer until the formation of a transparent solution. The above suspension was agitated for 1 h and centrifuged for 15 min at 7000 rpm. Eventually, the precipitate was washed repeatedly with deionized water and dried at 50 °C for 24 h (Orooji et al., 2020).

2.4. Bacterial isolates

In the present study, the antibacterial performance of Cu/g-C₃N₄ NCs (samples 1–4) was evaluated against isolates obtained from clinical samples the Shahid Beheshti hospital of Kashan, Iran (*Escherichia coli*, *Pseudomonas aeruginosa*, *Staphylococcus aureus*, *Enterococcus faecalis*, *Klebsiella pneumoniae*, and *Enterobacter cloacae*).

2.5. Antimicrobial activity

2.5.1. Measurement of the minimum inhibitory concentration (MIC)

The broth microdilution technique was used to evaluate the antibacterial performance of the Cu/g-C₃N₄ NCs (samples 1–

4) based on the Clinical and Laboratory Standards Institute (CLSI) standards. Mueller Hinton broth medium was added to 96-well microplate. Afterward, 100 µl of dispersed Cu/g-C₃N₄ NCs was added to each well to obtain a final concentration range from 2500 to 2.44 µg/mL by a series of two-fold dilutions. Then, bacterial suspension (1×10^7 CFU/mL) was diluted to obtain a final concentration 5×10^5 CFU/ml and was added to a 96-well plate. Next, the plate was incubated at 37 °C for 18–24 h. The MIC was determined as the lowest concentration of Cu/g-C₃N₄ at which no discernible growth was observed (Karami et al., 2021).

2.5.2. Measurement of the minimum bactericidal concentration (MBC)

The MBC was defined by plating 10 µl of the test solutions on the Blood Agar plate. The number of colonies was counted on the plate after 24 h. The MBC is the minimum concentration of the test compound needed to kill the bacteria (Karami et al., 2021).

2.5.3. Agar disk-diffusion approach

Disk diffusion test was applied to appraise the antimicrobial activity of the Cu/g-C₃N₄ NCs (samples 1–4). A sterile cotton

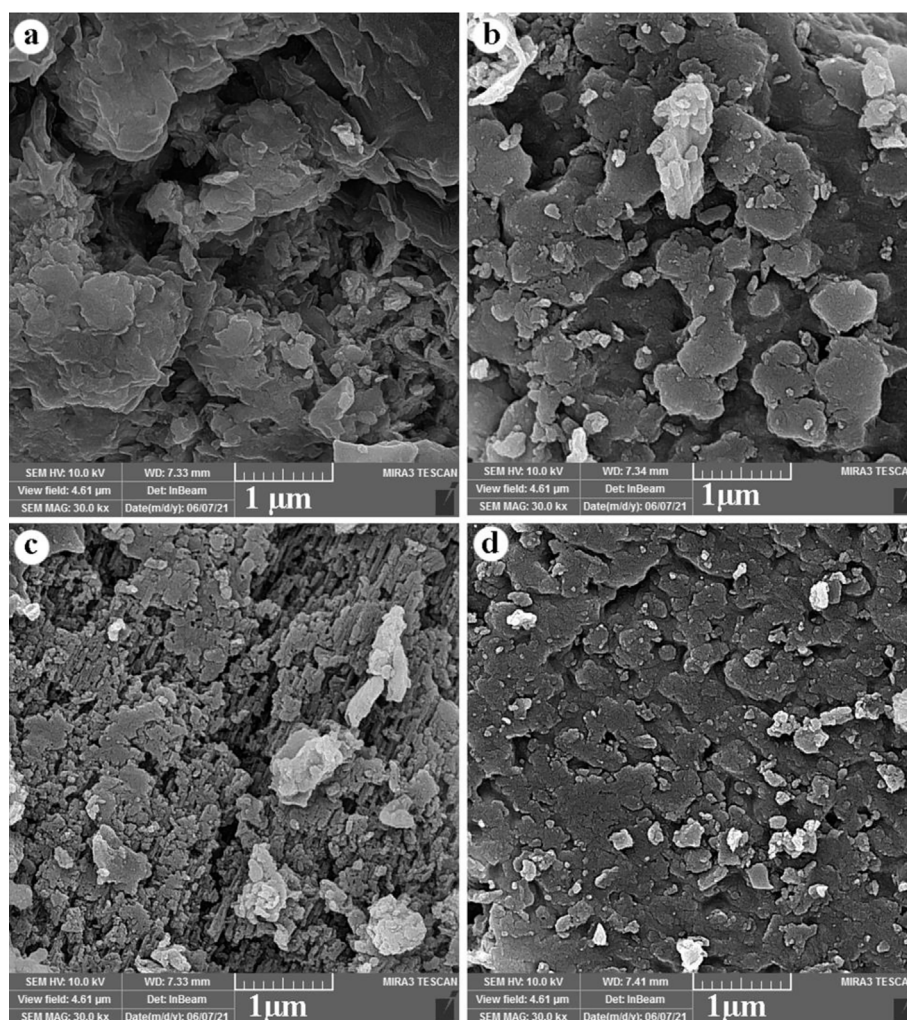


Fig. 3 FESEM images of Cu/g-C₃N₄ nanocomposites in different mass ratios a) 0.3:1, b) 0.4:1, c) 0.5:1, and d) 1:1.

swab was used to streak the bacterial suspension (1×10^7 CFU/mL) on the surface of the Muller Hinton agar. Then, sterile commercial blank disks were impregnated with samples 1–4 and placed on Muller Hinton agar and incubated at 37 °C for 24 h. The photographs of the plates were taken to evaluate the inhibition zone for the bacteria.

2.6. Biofilm formation assay

In this study, biofilm formation was evaluated using the microtiter plate method for all bacterial isolates. First, 100 μ l of bacterial suspension (10^7 CFU/ml) added to 96 well plates and incubated at 37 °C for 24 h. To eliminate non-adherence cells, wells washed with sodium phosphate buffer two times. We then applied methanol (200 μ l) for 20 min to fixation of attached cells. To stain the wells 0.1% crystal violet for 15 min was used. The dye was resuspended with 33% glacial acetic acid (200 μ l) (Maisetta et al., 2016; Rashki et al., 2022a). The absorbance value was obtained using a Microplate Reader at 570 nm. Based on absorbance values, bacterial isolates were classified into the following four groups: non-biofilm ($OD_{570} \leq OD_c$), weak ($OD_{570} > OD_c$ and $\leq 2 \times OD_c$), mod-

erate ($OD_{570} > 2 \times OD_c$ and $\leq 4 \times OD_c$), and strong ($OD_{570} > 4 \times OD_c$). The cutoff value (OD_c) is defined the mean OD_{570} of the negative control (Ghanizadeh et al., 2021).

2.7. Biofilm inhibition effect

We assessed the ability of Cu/g-C₃N₄ nanocomposite (sample 4) with MIC and sub-MIC (1/2 and 1/4) concentrations to inhibit the biofilm formation of isolates produced strong biofilm at 24 h using 96-well plates. For this purpose, 100 μ l bacterial suspension produced strong biofilm (1×10^7 CFU/mL) in Tryptic Soy Broth (TSB) medium (Merck, Germany) was seeded into 96-well plates in the presence of 100 μ l various concentrations of tests compounds and incubated at 37 °C for 24 h. After 24 h, wells were washed twice with phosphate-buffered saline (PBS) to remove non-adhered cells. The formed biofilms were fixed with methanol (20 min). The plate's wells were then stained with 0.1% (w/v) crystal violet for 15 min, and glacial acetic acid was used to re-solubilize crystal violet. After 15 min, the OD of each well was measured with a spectrophotometer at 570 nm. The following equation was used for the calculation of the inhibition percentage:

$$\left[1 - \left(\frac{A_{570} \text{ of cells treated with Cu/g-C}_3\text{N}_4}{570 \text{ of non-treated cells}} \right) \right] \times 100$$

2.8. Analysis of gene expression related to biofilm using real-time qPCR

In this research, we explored effect Cu/g-C₃N₄ NCs on the expression of *icaA* gene using real-time PCR method. Isolates that produced strong biofilm were chosen to assess gene expressions of *icaA*. First, RNA of the bacterial cells treated with sub-MIC (1/2 MIC) concentration was extracted with RNX Plus protocol. To assay purity of the extracted RNA, the absorbance of RNA was measured at 260 and 280 nm by UV spectroscopy (Thermo Scientific, USA). Then, the cDNA (complementary DNA) was synthesized based on kit (*Pars Tous, Iran*) guidelines. The primer sequences and reference gene (*glyA gene*) were listed in Table 1. The fold change was normalized according to the $2^{-\Delta\Delta CT}$ formula.

3. Results and discussion

3.1. Characterization

Fig. 1 reveals the XRD patterns of pure Cu NPs, pristine g-C₃N₄ and Cu/g-C₃N₄ nanocomposites with different mass ratios. Fig. 1a depicts high purity and crystallinity of Cu

(JCPDS No. 085-1326). Fig. 1b shows the pattern of carbon nitride (JCPDS No. 87-1526), exhibiting two distinct peaks. The sharpest one, occurring at 26.5°, and the smallest one, at 13.1°, are indexed as (002) and (001) planes of C₃N₄, respectively. Fig. 1(c-f) indicates the XRD patterns of different contents of Cu on the g-C₃N₄. Cu (JCPDS No. 085-1326) and g-C₃N₄ (JCPDS No. 87-1526) are present in all four patterns. As can be seen, increasing the Cu content from 0.3 g to 1.0 g decreased the intensity of carbon nitride while increasing the intensity of Cu peaks.

The FESEM images of Cu particles fabricated with and without SDS as a surfactant are depicted in Fig. 2. Fig. 2a and b display regular pyramidal particles composed in the presence of SDS, while the irregular triangular particles were formed in the absence of SDS (Fig. 2c and d). Cu particles in the presence of SDS have better morphology; therefore, SDS was used in the further tests to prepare Cu/g-C₃N₄ nanocomposites. SDS can affect the regularity and distribution of copper particles in certain conditions. SDS is a commonly used surfactant in various chemical and biological applications due to its ability to reduce surface tension and stabilize colloidal suspensions. When added to a copper particle solution, SDS molecules can adsorb onto the surface of the particles and form a protective layer, preventing agglomeration and promoting dispersion. This can lead to more uniform distribution of copper particles in the solution. Fig. 3(a-d) reveals the FESEM photographs of Cu/g-C₃N₄ NPs with various mass ratios. These images demonstrate the nanoflake architecture of g-

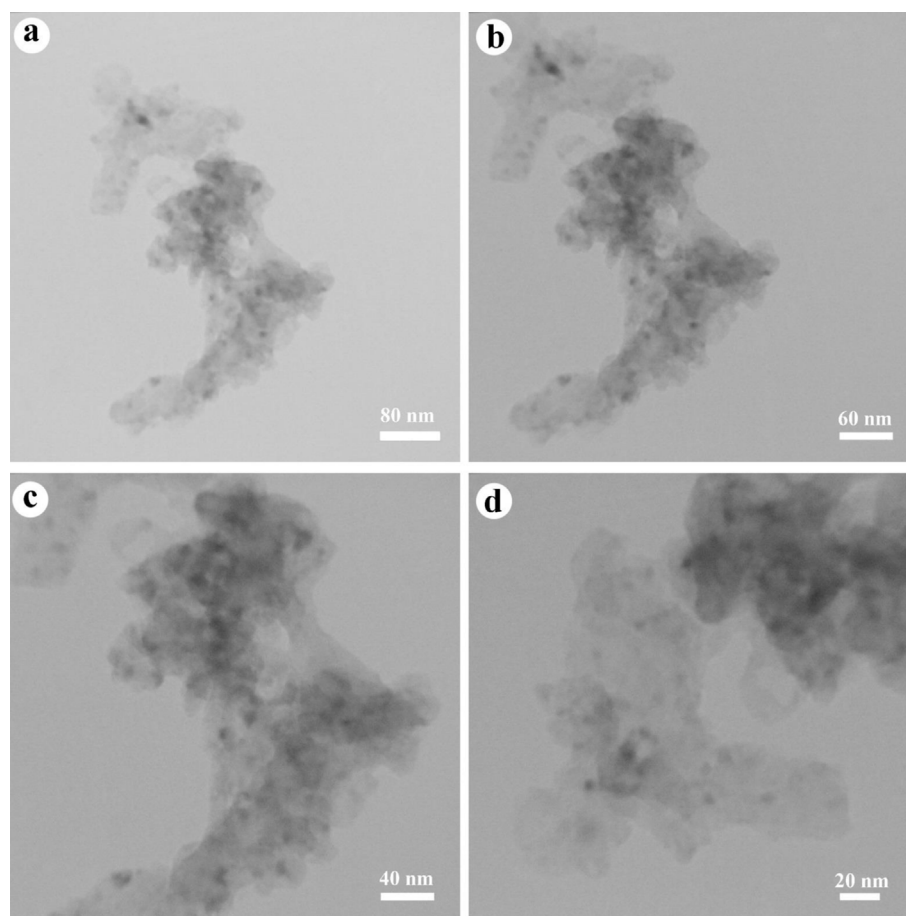


Fig. 4 TEM images of Cu/g-C₃N₄ nanocomposites (sample 4).

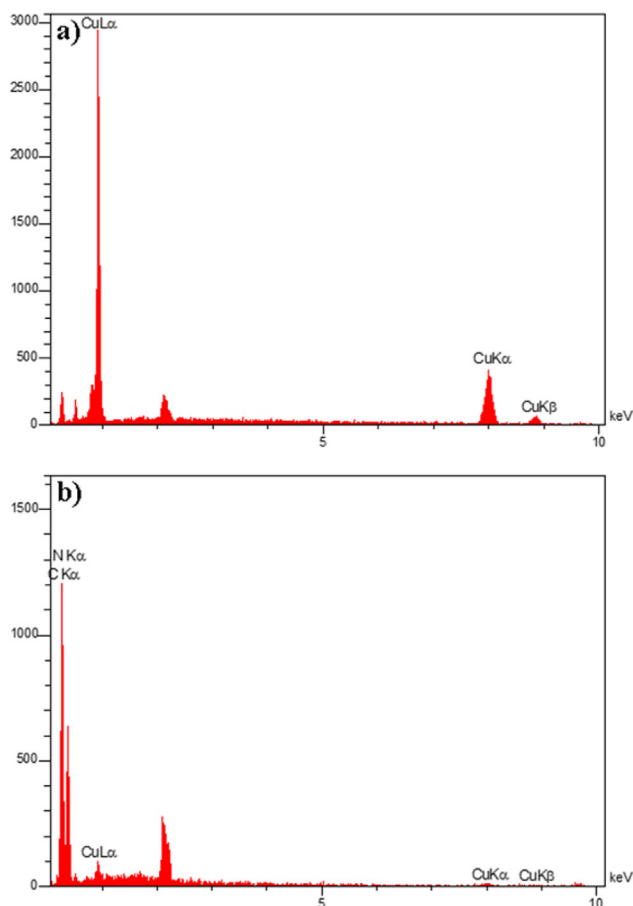


Fig. 5 EDS spectra of a) Cu and b) Cu/g-C₃N₄ nanocomposites.

C₃N₄ and Cu NPs arranged on the g-C₃N₄ surface. Typically, expanding the quantity of Cu leads to an accumulation in the diameter of Cu NPs on the carbon nitride surface. Fig. 4(a-d) shows TEM images of sample 4 with a 1:1 mass ratio of Cu:g-C₃N₄ at various scales (80, 60, 40, and 20 nm). These pictures corroborated the FESEM findings and demonstrated the distribution of Cu NPs on the g-C₃N₄ substrate. EDS spectroscopy is a scientific method used for chemical description and elemental analysis of materials. Fig. 5a and b depict the EDS spectra of Cu and Cu/g-C₃N₄, representing all peaks allocated to Cu, C, and N elements. Therefore, both samples are thoroughly purified.

3.2. Antimicrobial activity

In this study, the antimicrobial activity of Cu/g-C₃N₄ NCs, and g-C₃N₄ was evaluated by the broth microdilution method. As revealed in Table 2, samples 3 and 4 (with higher Cu content) were more effective against the tested bacterial species than other samples. Also, the results demonstrated that these samples were more effective against gram-positive than gram-negative bacteria. According to the results, the loaded Cu-NPs on the g-C₃N₄ could improve its antibacterial activity. Furthermore, according to MIC values, we understand that sample 4 could inhibit the growth of test bacteria in lower concentrations compared to other samples. In this study, the inhibition zone diameters of tested bacteria using disk diffusion method. Table 3 and Fig. 6. The results showed that sample 4 had larger inhibition zone than the other samples. The inhibitory growth zone of *Staphylococcus aureus* (29 mm) is greater than that of the other microorganisms tested. According to research, the presence of Cu NPs is

Table 2 The Minimum Inhibitory Concentration (MIC) and Minimum Bactericidal Concentration (MBC) of nanostructures against tested microorganisms.

Bacteria	Cu/g-C ₃ N ₄ NCs				g-C ₃ N ₄	
	Sample 3		Sample 4		MIC	MBC
	MIC	MBC	MIC	MBC		
<i>Staphylococcus aureus</i>	1250	1250	312.5	2500	–	–
<i>Enterococcus faecalis</i>	–	–	–	–	–	–
<i>Escherichia coli</i>	1250	2500	625	1250	–	–
<i>Pseudomonas aeruginosa</i>	1250	1250	1250	2500	–	–
<i>Klebsiella pneumonia</i>	–	–	–	–	–	–
<i>Enterobacter cloacea</i>	–	–	1250	5000	–	–

Table 3 The inhibition zones (mm) of Cu/ g-C₃N₄ NCs (sample 3, 4) against tested microorganisms.

Bacteria	Sample 3	Sample 4
<i>Staphylococcus aureus</i>	14	29
<i>Enterococcus faecalis</i>	–	–
<i>Escherichia coli</i>	11	15
<i>Pseudomonas aeruginosa</i>	10	19
<i>Klebsiella pneumonia</i>	–	–
<i>Enterobacter cloacea</i>	12	16

responsible for the antibacterial activity of Cu/g-C₃N₄ NCs (Sun et al., 2017). The exact mechanism of antibacterial activity is not fully understood, and several other factors may contribute to the antibacterial action (Sun et al., 2017; Thurston et al., 2020). According to studies, the surface of Cu NPs plays a crucial role in antibacterial activity. Copper antibacterial functionality is associated with various mechanisms, including damaging the microbial DNA, altering bacterial protein synthesis and altering membrane integrity. Some research has evaluated the antibacterial activity of the loaded nanoparticles on the g-C₃N₄. For instance, Orooji et al. investigated the antibacterial action of silver iodide/graphitic carbon nitride nanocomposites against tested bacteria. The results demonstrated that silver iodide could enhance the g-C₃N₄ antibacterial effect (Orooji et al., 2020). In a study by Chongchong et al., the g-C₃N₄/Ag nanocomposites showed better bacterial activity than g-C₃N₄ (Liu et al., 2016). The findings of this research are similar to the results of the present study. It can be confirmed that the loaded nanoparticles on the g-C₃N₄ can enhance the antibacterial performance of the g-C₃N₄. (Cabisco Català et al., 2000; Thurston et al., 2020). It is concluded that Cu NPs have the potential to enhance the antibacterial effect of g-C₃N₄ against resistant pathogenic microbes.

3.3. Antibiofilm activity

Biofilm formation is the main cause of chronic bacterial infections and could lead to an increase in antibiotic resistance. Preformed biofilm by blocking the diffusion of antimicrobial agents into the biofilm matrix could enhance the resistance of bacteria (Abebe, 2020). In this study, only *S. aureus* isolates were strong biofilm producers. Therefore, in this study, we assayed the ability of Cu/g-C₃N₄ NCs (sample 4) to inhibit the formation of biofilms of *S. aureus* at 24 h. The results

demonstrated that Cu/g-C₃N₄ NCs significantly inhibited biofilm formation of *S. aureus* strain in a concentration-dependent manner. As quantified by crystal violet, Cu/g-C₃N₄ inhibited biofilm formation in the *S. aureus* strain by 65% at the MIC concentration (Fig. 7). Given that the extracellular matrix is a major structural component of microbial biofilms (Karygianni et al., 2020). One of the main reasons for the effect of Cu-NPs on inhibited biofilm formation in the *S. aureus* is their particle size, as smaller particles with large surface area have more interaction with extracellular matrix bacteria. So that by destroying the extracellular matrix leads to the weakening of the biofilm and facilitates the entry of the drug into the inner layer of the biofilm (Bi et al., 2021).

3.4. Analysis of *icaA* gene expression in the presence of Cu/g-C₃N₄ nanocomposites using Real-time qPCR

To further understand the antibiofilm mechanism of prepared Cu/g-C₃N₄ NCs, change the gene expression related to biofilm *S. aureus* in the presence of this nanocomposites was evaluated. For this purpose, we compared the expression of *icaA* gene in *S. aureus* isolated after treatment with prepared nanocomposite by RT-PCR technique. So far, there is no similar study has been evaluated the effects of Cu/g-C₃N₄ NCs on the expression of this gene. In other words, we assessed the expression of *icaA* genes for the first time. As shown in Fig. 8, following treatment with Cu/g-C₃N₄ NCs, the expression level of the *icaA* gene was down-regulated as much as 2.26. Although, the expressions of *icaA* gene in isolates treated with antibiotic decreased by 6 folds. In general, antibiotic has reduced gene expression more than Cu/g-C₃N₄ NCs. The exact mechanism of this phenomenon is still unclear. Generally, *icaA* gene facilitate bacterial attachment to the surfaces and as a result, leading the formation of biofilm. Therefore, the factors that cause changes in the expression level of this gene can help

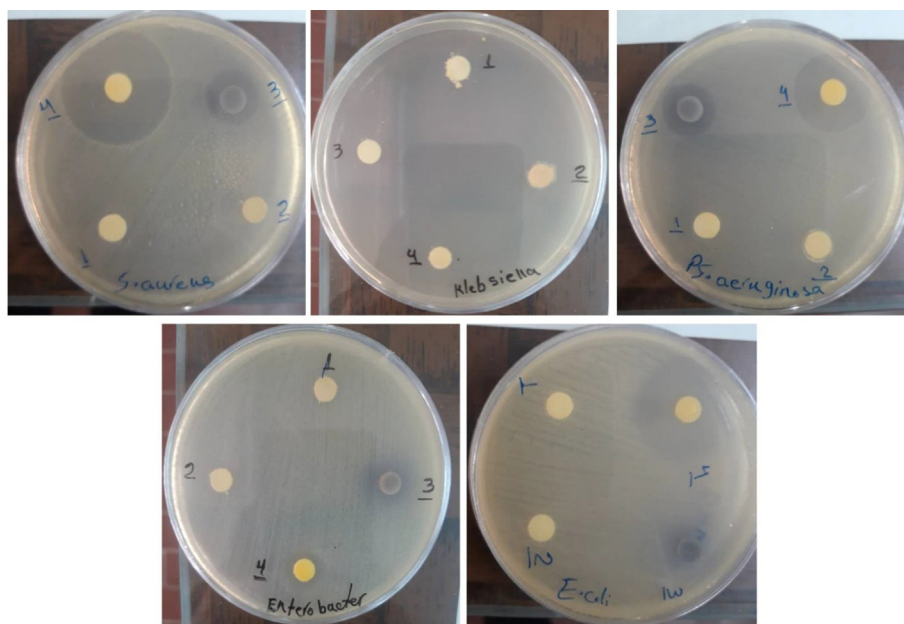


Fig. 6 Zones of growth inhibition of Cu/g-C₃N₄ nanocomposites (samples 1, 2, 3, and 4) on tested microorganisms *S. aureus*, *klebsiella pneumoniae*, *pseudomonas aeruginosa*, *Enterobacter cloacea* and, *Escherichia coli*.

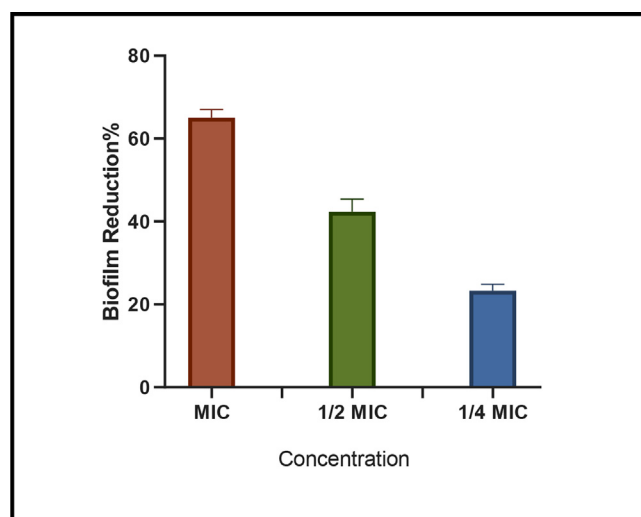


Fig. 7 Effect of Cu/g-C₃N₄-NCs (sample 4) at MIC, \emptyset MIC and $\frac{1}{4}$ MIC concentration on the formation of *Staphylococcus aureus* biofilm analyzed via crystal violet staining.

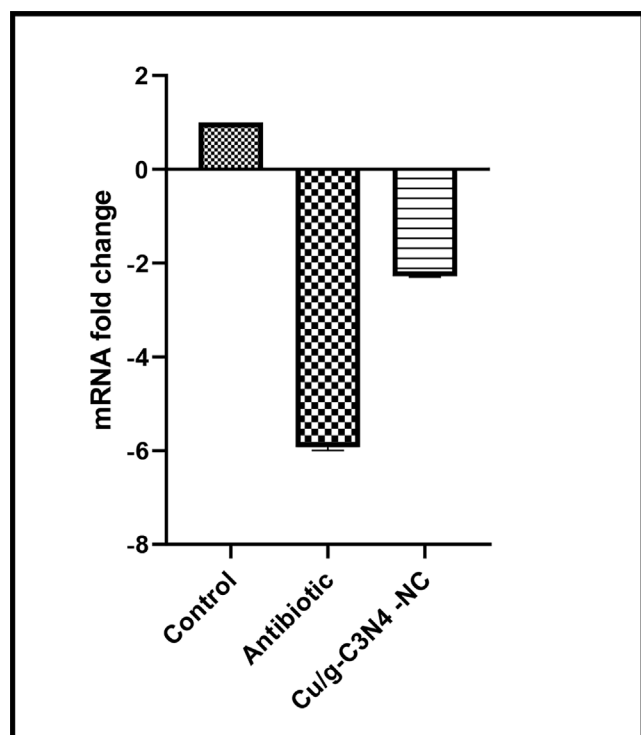


Fig. 8 The effect of Cu/g-C₃N₄-NCs on *icaA* gene expression. All graphs represent mean SEM.

to reduce biofilm formation. Thereby Cu/g-C₃N₄ NCs with reduced *icaA* expression can have an impact important on the biofilm inhibition of *S. aureus*.

4. Conclusion

Our results showed that the doping of Cu-NPs with graphitic carbon nitride can lead to an improved antibacterial activity of g-C₃N₄. So,

Cu/g-C₃N₄ nanocomposite is more effective against tested gram-positive and gram-negative bacteria, especially *S. aureus*. Also, this nanocomposite could be used to reduce or prevent biofilm formation on medical devices. The biofilm inhibition in *S. aureus* isolate was *icaA* gene independent as a result of down-regulation of *icaA* gene led to biofilm inhibition in *S. aureus* after treatment by Cu/g-C₃N₄ nanocomposite. Therefore, Cu/g-C₃N₄ could be applied for the treatment of medical device-related infections. Given the potential of Cu/g-C₃N₄ as a promising antimicrobial and antibiofilm material could be utilized to reduce antibacterial resistance among clinical isolates. This compound has the potential to prevent or treat pathogen-caused infections.

CRedit authorship contribution statement

Somaye Rashki: Software, Investigation, Methodology, Formal analysis. **Mojgan Ghanbari:** Writing – review & editing, Writing – original draft, Software. **Zainab Hashim Khudhair:** Writing – review & editing, Data curation. **Zeynab Marzho-seyni:** Software, Data curation, Visualization. **Zakaria Bameri:** Software, Data curation, Validation. **Saleh Afsharikhah:** Software, Conceptualization, Data curation, Validation. **Waleed K. Abdulsahib:** Writing – review & editing, Data curation. **Ali Nazari-Alam:** Software, Funding acquisition, Data curation, Validation. **Masoud Salavati-Niasari:** Formal analysis, Methodology, Writing – review & editing, Writing – original draft, Conceptualization, Methodology, Supervision, Project administration, Investigation, Data curation, Validation, Resources, Visualization, Funding acquisition.

Declaration of Competing Interest

The authors declare that they have no known competing financial interests or personal relationships that could have appeared to influence the work reported in this paper.

References

- Abdulhusain, Z.H., Mahdi, M.A., Abdulsahib, W.K., Jasim, L.S., 2022. Anabasis articulata exerts an anti-arthritis effect on adjuvant-induced arthritis in rats. *J. Adv. Pharm. Technol. Res.* 13 (4), 276–280. https://doi.org/10.4103/japtr.japtr_440_22.
- Abebe, G.M., 2020. The role of bacterial biofilm in antibiotic resistance and food contamination. *Int. J. Microbiol.* 2020, 1705814. <https://doi.org/10.1155/2020/1705814>.
- Begletsova, N., Selifonova, E., Chumakov, A., Al-Alwani, A., Zakharevich, A., Chernova, R., Glukhovskoy, E., 2018. Chemical synthesis of copper nanoparticles in aqueous solutions in the presence of anionic surfactant sodium dodecyl sulfate. *Colloids Surf A Physicochem Eng Asp* 552, 75–80.
- Bi, Y., Xia, G., Shi, C., Wan, J., Liu, L., Chen, Y., Wu, Y., Zhang, W., Zhou, M., He, H., 2021. Therapeutic strategies against bacterial biofilms. *Fundam. Res.* 1 (2), 193–212.
- Cabiscol Català, E., Tamarit Sumalla, J., Ros Salvador, J., 2000. Oxidative stress in bacteria and protein damage by reactive oxygen species. *Int. Microbiol.* 3 (1), 3–8.
- Cheng, X., Zhang, X., Yin, H., Wang, A., Xu, Y., 2006. Modifier effects on chemical reduction synthesis of nanostructured copper. *Appl. Surf. Sci.* 253 (5), 2727–2732.
- Cucarella, C., Solano, C., Valle, J., Amorena, B., Lasa, I.N.I., Penadés, J.R., 2001. Bap, a *Staphylococcus aureus* surface protein involved in biofilm formation. *J. Bacteriol.* 183 (9), 2888–2896.
- Deng, J., Liang, J., Li, M., Tong, M., 2017. Enhanced visible-light-driven photocatalytic bacteria disinfection by g-C₃N₄-AgBr. *Colloids Surf. B Biointerfaces* 152, 49–57.

- Gajdacs, M., Baráth, Z., Kárpáti, K., Szabó, D., Usai, D., Zanetti, S., Donadu, M.G., 2021. No correlation between biofilm formation, virulence factors, and antibiotic resistance in *Pseudomonas aeruginosa*: results from a laboratory-based in vitro study. *Antibiotics* 10 (9), 1134.
- Ghanizadeh, A., Najafizade, M., Rashki, S., Marzhoseyni, Z., Motallebi, M., 2021. Genetic diversity, antimicrobial resistance pattern, and biofilm formation in *Klebsiella pneumoniae* isolated from patients with coronavirus disease 2019 (COVID-19) and ventilator-associated pneumonia. *Biomed Res. Int.* 2021. <https://doi.org/10.1155/2021/2347872>.
- Giraldi, G., Montesano, M., Napoli, C., Frati, P., La Russa, R., Santurro, A., Scopetti, M., Orsi, G.B., 2019. Healthcare-associated infections due to multidrug-resistant organisms: a surveillance study on extra hospital stay and direct costs. *Curr. Pharm. Biotechnol.* 20 (8), 643–652.
- Huang, J., Ho, W., Wang, X., 2014. Metal-free disinfection effects induced by graphitic carbon nitride polymers under visible light illumination. *Chem. Commun.* 50 (33), 4338–4340.
- Karami, M., Ghanbari, M., Alshamsi, H.A., Rashki, S., Salavati-Niasari, M., 2021. Facile fabrication of Ti 4 HgI 6 nanostructures as novel antibacterial and antibiofilm agents and photocatalysts in the degradation of organic pollutants. *Inorg. Chem. Front.* 8 (10), 2442–2460.
- Karygianni, L., Ren, Z., Koo, H., Thurnheer, T., 2020. Biofilm matrixome: extracellular components in structured microbial communities. *Trends Microbiol.* 28 (8), 668–681.
- Li, G., Nie, X., Chen, J., Jiang, Q., An, T., Wong, P.K., Zhang, H., Zhao, H., Yamashita, H., 2015. Enhanced visible-light-driven photocatalytic inactivation of *Escherichia coli* using g-C₃N₄/TiO₂ hybrid photocatalyst synthesized using a hydrothermal-calcination approach. *Water Res.* 86, 17–24.
- Li, R., Ren, Y., Zhao, P., Wang, J., Liu, J., Zhang, Y., 2019. Graphitic carbon nitride (g-C₃N₄) nanosheets functionalized composite membrane with self-cleaning and antibacterial performance. *J. Hazard. Mater.* 365, 606–614.
- Liu, C., Wang, L., Xu, H., Wang, S., Gao, S., Ji, X., Xu, Q., Lan, W., 2016. “One pot” green synthesis and the antibacterial activity of g-C₃N₄/Ag nanocomposites. *Mater. Lett.* 164, 567–570.
- Ma, S., Zhan, S., Jia, Y., Shi, Q., Zhou, Q., 2016. Enhanced disinfection application of Ag-modified g-C₃N₄ composite under visible light. *Appl Catal B* 186, 77–87.
- Mahde, B.W., Sultan, A.M., Mahdi, M.A., Jasim, L.S., 2022. Kinetic adsorption and release study of sulfadiazine hydrochloride drug from aqueous solutions on GO/P(AA-AM-MCC) composite. *Int. J. Drug Deliv. Technol.* 12 (4), 1583–1589. <https://doi.org/10.25258/ijddt.12.4.17>.
- Maisetta, G., Grassi, L., Di Luca, M., Bombardelli, S., Medici, C., Brancatisano, F.L., Esin, S., Batoni, G., 2016. Anti-biofilm properties of the antimicrobial peptide temporin 1Tb and its ability, in combination with EDTA, to eradicate *Staphylococcus epidermidis* biofilms on silicone catheters. *Biofouling* 32 (7), 787–800.
- Murugesan, P., Narayanan, S., Matheswaran, M., 2018. Photocatalytic performance and antibacterial activity of visible light driven silver iodide anchored on Graphitic-C₃N₄ binary composite. *Environ. Nanotechnol. Monit. Manage.* 10, 253–263.
- Naseri, A., Samadi, M., Pourjavadi, A., Moshfegh, A.Z., Ramakrishna, S., 2017. Graphitic carbon nitride (gC₃N₄)-based photocatalysts for solar hydrogen generation: recent advances and future development directions. *J. Mater. Chem. A* 5 (45), 23406–23433.
- Orooji, Y., Ghanbari, M., Amiri, O., Salavati-Niasari, M., 2020. Facile fabrication of silver iodide/graphitic carbon nitride nanocomposites by notable photo-catalytic performance through sunlight and antimicrobial activity. *J. Hazard. Mater.* 389, 122079.
- Oves, M., Ansari, M.O., Darwesh, R., Hussian, A., Alajmi, M.F., Qari, H.A., 2020. Synthesis and antibacterial aspects of graphitic C₃N₄@ polyaniline composites. *Coatings* 10 (10), 950.
- Rashki, S., Safardoust-Hojaghan, H., Mirzaei, H., Abdulsahib, W.K., Mahdi, M.A., Salavati-Niasari, M., Khaledi, A., Khorshidi, A., Mousavi, S.G.A., 2022a. Delivery LL37 by chitosan nanoparticles for enhanced antibacterial and antibiofilm efficacy. *Carbohydrate Polym.* 291. <https://doi.org/10.1016/j.carbpol.2022.119634>.
- Sert, B., Ozay, Y., Harputlu, E., Ozdemir, S., Yalcin, M.S., Ocakoglu, K., Dizge, N., 2021. Improvement in performance of g-C₃N₄ nanosheets blended PES ultrafiltration membranes including biological properties. *Colloids Surf. A Physicochem. Eng. Asp* 623, 126571.
- Sun, L., Du, T., Hu, C., Chen, J., Lu, J., Lu, Z., Han, H., 2017. Antibacterial activity of graphene oxide/g-C₃N₄ composite through photocatalytic disinfection under visible light. *ACS Sustain. Chem. Eng.* 5 (10), 8693–8701.
- Thurston, J.H., Clifford, A.J., Henderson, B.S., Smith, T.R., Quintana, D., Cudworth, K.F., Lujan, T.J., Cornell, K.A., 2020. Development of photoactive g-C₃N₄/poly (vinyl alcohol) composite hydrogel films with antimicrobial and antibiofilm activity. *ACS Appl. Bio Mater.* 3 (3), 1681–1689.
- Wang, T., Nie, C., Ao, Z., Wang, S., An, T., 2020. Recent progress in gC₃N₄ quantum dots: synthesis, properties and applications in photocatalytic degradation of organic pollutants. *J. Mater. Chem. A* 8 (2), 485–502.
- Xu, M., Yang, G., Bi, H., Xu, J., Feng, L., Yang, D., Sun, Q., Gai, S., He, F., Dai, Y., 2019. Combination of CuS and g-C₃N₄ QDs on upconversion nanoparticles for targeted photothermal and photodynamic cancer therapy. *Chem. Eng. J.* 360, 866–878.
- Yousefzadeh, F., Yousif, Q.A., Ghanbari, M., Salavati-Niasari, M., 2022. Fabrication of TiSnI₃/C₃N₄ nanocomposites for enhanced photodegradation of toxic contaminants below visible light and investigation of kinetic and mechanism of photocatalytic reaction. *J. Mol. Liquids* 349. <https://doi.org/10.1016/j.molliq.2021.118443>.
- Zhang, Y., Chan, H.F., Leong, K.W., 2013. Advanced materials and processing for drug delivery: the past and the future. *Adv. Drug Deliv. Rev.* 65 (1), 104–120.
- Zhou, L., Wang, L., Zhang, J., Lei, J., Liu, Y., 2016. Well-Dispersed Fe₂O₃ nanoparticles on g-C₃N₄ for efficient and stable photocatalysis under visible-light irradiation. *Eur. J. Inorg. Chem.* 2016 (34), 5387–5392.